

THE STAR FORMATION RATE AND METALLICITY OF THE HOST GALAXY OF THE DARK GRB 080325 AT $z = 1.78$

TETSUYA HASHIMOTO¹, DANIEL A. PERLEY², KOUJI OHTA³, KENTARO AOKI⁴, ICHI TANAKA⁴,
YUU NIINO¹, KIYOTO YABE¹, AND NOBUYUKI KAWAI⁵

¹ National Astronomical Observatory of Japan, 2-21-1 Osawa, Mitaka, Tokyo 181-8588, Japan

² Department of Astronomy, California Institute of Technology, MC 249-17, 1200 East California Boulevard, Pasadena, CA 91125, USA

³ Department of Astronomy, Kyoto University, Kyoto 606-8502, Japan

⁴ Subaru Telescope, National Astronomical Observatory of Japan, 650 North A'ohoku Place, Hilo, HI 96720, USA

⁵ Department of Physics, Tokyo Institute of Technology, 2-12-1 Ookayama, Meguro-ku, Tokyo 152-8551, Japan

Received 2014 November 11; accepted 2015 March 23; published 2015 June 22

ABSTRACT

We present near-infrared spectroscopy of the host galaxy of the dark gamma-ray burst (GRB) 080325 using Subaru/Multi-Object Infrared Camera and Spectrograph. The obtained spectrum provides a clear detection of H α emission and marginal [NII] λ 6584. The host is a massive ($M_* \sim 10^{11} M_\odot$), dusty ($A_V \sim 1.2$) star-forming galaxy at $z = 1.78$. The extinction-corrected star formation rate (SFR) calculated from the H α luminosity ($35.6\text{--}47.0 M_\odot \text{ yr}^{-1}$) is typical among GRB host galaxies (and star-forming galaxies generally) at $z > 1$; however, the specific SFR is lower than for normal star-forming galaxies at redshift ~ 1.6 , in contrast to the high specific SFR measured for many of other GRB hosts. The metallicity of the host is estimated to be $12 + \log(\text{O}/\text{H})_{\text{KK04}} = 8.88$. We emphasize that this is one of the most massive host galaxies at $z > 1$ for which metallicity is measured with emission-line diagnostics. The metallicity is fairly high among GRB hosts, however, this is still lower than the metallicity of normal star-forming galaxies of the same mass at $z \sim 1.6$. The metallicity offset from normal star-forming galaxies is close to a typical value of other GRB hosts and indicates that GRB host galaxies are uniformly biased toward low metallicity over a wide range of redshifts and stellar masses. The low-metallicity nature of the GRB 080325 host likely cannot be attributed to the fundamental metallicity relation of star-forming galaxies because it is a metal-poor outlier from the relation and has a low specific star formation rate. Thus, we conclude that metallicity is important to the mechanism that produced this GRB.

Key words: galaxies: abundances – gamma-ray burst: individual (GRB 080325)

1. INTRODUCTION

Long-duration gamma-ray bursts (hereafter, GRBs) are among the most energetic phenomena in the universe. The extremely luminous optical afterglows associated with these explosions can be bright enough to be visible even with the naked eye (e.g., Racusin et al. 2008) and are observable at very high redshifts ($z > 6$ and beyond, e.g., Kawai et al. 2006; Salvaterra et al. 2009; Tanvir et al. 2009). While it is now widely accepted that GRBs originate from the deaths of massive stars, the identity of the progenitor and the evolutionary pathway required to produce it remain a matter of discussion. Some theoretical models of this process involving the evolution of a single, rapidly rotating massive star (e.g., Woosley & Heger 2006; Yoon et al. 2006) require a low-metallicity environment, a possibility which can be tested by examining the properties of the host galaxy population. Indeed, many low- z GRB host galaxies are low-luminosity and show blue colors (e.g., Le Floc'h et al. 2003), suggesting that they are metal-poor, given the mass–metallicity relationship for star-forming galaxies (e.g., Tremonti et al. 2004; Erb et al. 2006; Hayashi et al. 2009; Yabe et al. 2012, 2014). Spectroscopic observations of many of these GRB host galaxies confirm their low metallicities (e.g., Stanek et al. 2006; Modjaz et al. 2008).

However, several examples of more massive, red GRB hosts have also been reported in recent years (e.g., Berger et al. 2007; Hashimoto et al. 2010; Hunt et al. 2011; Krühler et al. 2011; Svensson et al. 2012; Perley et al. 2013), most of which are associated with “dark” GRBs (Jakobsson et al. 2004). This

hints at the possibility of a high-metallicity environment for at least some GRBs. In fact, high metallicities have been reported for a few cases based on emission-line diagnostics (Levesque et al. 2010b; Niino et al. 2012; Elliott et al. 2013; Graham & Fruchter 2013; Schulze et al. 2014; Stanway et al. 2015). These high-metallicity hosts seem to contradict models in which the GRB progenitor can *only* form in metal-poor environments. However, the average metallicity of a host galaxy does not necessarily reflect the metallicity of the GRB explosion site (Levesque et al. 2010b; Niino 2011; Schulze et al. 2014; Niino et al. 2014). Metallicity measurements of both the host galaxy and the GRB explosion site are important to reveal a complete picture of GRB origins.

GRB 080325 is a dark GRB whose near-infrared (NIR) afterglow and host galaxy were found through a target-of-opportunity program with the Subaru telescope (Tanaka et al. 2008). The host is a red, massive ($\sim 10^{11} M_\odot$) galaxy at $z_{\text{phot}} \sim 1.9$, as previously estimated by spectral energy distribution (SED) fitting analysis (Hashimoto et al. 2010). Thus, this GRB host serves as good test case to investigate the influence of physical environment in producing GRBs in the high-redshift universe.

This paper is organized as follows. We present our NIR spectroscopy of the GRB 080325 host galaxy and spectral analysis in Section 2 and briefly describe the results of our analysis in Section 3. In Section 4, we discuss properties of the GRB 080325 host galaxy, focusing in particular on the star formation rate (SFR) and metallicity and their variation between possible multiple components of the host. Finally, our results and discussions are summarized in Section 5.

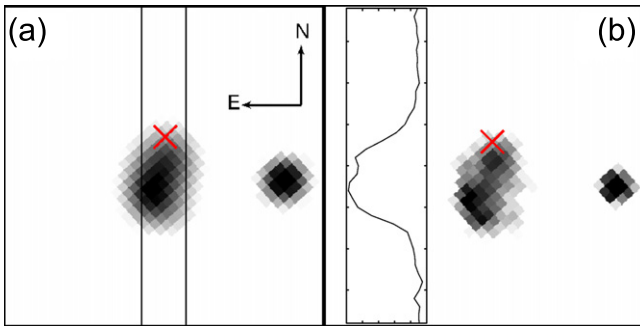


Figure 1. *HST*/WFC3 *J*-band images ($5''0 \times 5''0$) of the GRB 080325 host galaxy along with a neighboring point source. Image (a) is smoothed to have a seeing size of $\sim 0''.6$ (the typical seeing during Subaru spectroscopic observations) for the purpose of the slit loss estimate. The red cross represents the position of the GRB afterglow (Tanaka et al. 2008). The two black lines represent the position of the Subaru/MOIRCS $0''.7$ slit. Image (b) is the original *HST*/WFC3 *J*-band image with FWHM $\sim 0''.29$ along with a north-south profile of the surface brightness of the host.

Throughout this paper, we use cosmological parameters of $H_0 = 70.0 \text{ km s}^{-1} \text{ Mpc}^{-1}$, $\Omega_M = 0.279$, and $\Omega_\Lambda = 0.721$ (Bennett et al. 2013).

2. NEAR-INFRARED SPECTROSCOPY OF GRB 080325 HOST

We obtained a spectrum of the host galaxy of GRB 080325 using the Subaru/Multi-Object Infrared Camera and Spectrograph (MOIRCS; Ichikawa et al. 2006; Suzuki et al. 2008) HK500 grism covering $1.3\text{--}2.5 \mu\text{m}$ as well as a standard star FS147 (A0) on 2011 June 22 and 23. Weather conditions were clear throughout the observation. The seeing varied between approximately $0''.5$ and $0''.8$ in the K_s band. The slit ($0''.7$ width) was oriented to cover a large part of the host galaxy, as shown in Figure 1(a); this provides a resolving power of $R = 630$ at $1.8 \mu\text{m}$ measured from sky emission lines. A standard ABAB sequence was employed to subtract OH sky emission lines with a total 7 hr exposure on source.

We detected a strong, spatially and spectrally resolved emission line at a wavelength of $\lambda = 18243.4 \text{ \AA}$, as well as faint continuum at the expected position of the host galaxy (Figure 2). We associate this line with $\text{H}\alpha$ at $z = 1.78$ on the basis of the absence of any other strong lines in our spectral range, a probable detection of $[\text{NII}]\lambda 6584$ at the appropriate wavelength, and its good consistency with the photometric redshift measurement (see Section 4.3 for additional discussion). The GRB position is denoted by an upper horizontal dashed line in Figure 2, which is calculated from the offset distance between the afterglow and the center of the host galaxy (Hashimoto et al. 2010). The morphology of the $\text{H}\alpha$ line in the 2D spectrum shows a redshifted component around the GRB position. We divided the spectrum into the “south” and redshifted “north” parts. The boundary between the two is denoted by a bottom horizontal dashed line in Figure 2. The extraction windows are $1''.4$ and $1''.1$, respectively. These two spectra roughly correspond to the two resolved components of the host galaxy seen in the *J*-band image from the *Hubble Space Telescope* (*HST*) obtained by Perley et al. (2013) as shown in Figure 1(b). We also simply summed these two spectra to extract the “whole” spectrum of the host according to the conventional manner adopted by many other previous GRB host studies.

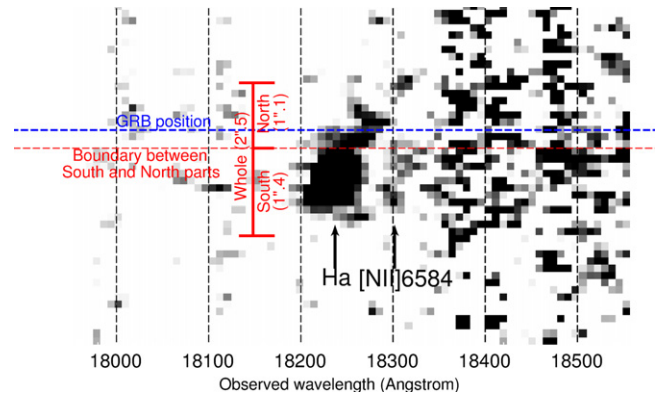


Figure 2. 2D spectrum of the GRB 080325 host galaxy obtained by MOIRCS/HK500 grism. The blue horizontal line corresponds to the position of the afterglow reported by Tanaka et al. (2008). Red arrows show the extracted regions used to make one-dimensional spectra.

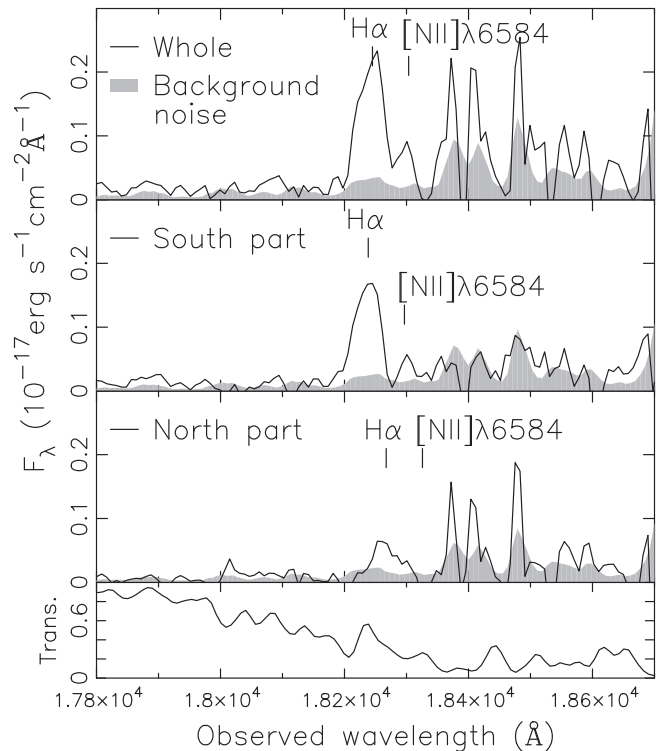


Figure 3. Spectra of GRB 080325 host galaxy extracted from the Whole, north, and south parts as shown in Figure 2 and atmospheric transparency measured from a telluric standard star (bottom). The filled gray area shows the 1σ background noise estimated from the off-source region along the slit length. $\text{H}\alpha$ position and corresponding $[\text{NII}]\lambda 6584$ are marked with vertical lines. The pixel scale for the spectra is $7.93 \text{ \AA pix}^{-1}$.

Figure 3 shows spectra extracted from the whole, south, and north parts of the host galaxy along with the 1σ background noise which is estimated from an off-source region along the slit length. The redshift of the GRB 080325 host is 1.7797 ± 0.0001 as derived from the Whole spectrum, which provides good agreement with the original photometric redshift within fitting uncertainties (Hashimoto et al. 2010). The $\text{H}\alpha$ wavelength in the south spectrum corresponds to $z = 1.7786 \pm 0.0001$. Although the signal-to-noise ratio (S/N) of $\text{H}\alpha$ in the north spectrum is poor, the redshift of the north part is estimated to be 1.7831 ± 0.0003 . The redshift uncertainties described above are from spectral fitting errors. Although

redshift measurements also contain additional systematic errors of 0.0025 from the slit alignment of the host galaxy, they do not affect the velocity offset between the two components because the two move in a parallel manner. We also marginally detected the [NII] λ 6584 line for the whole and south part of the spectra at about 3σ significance. We note that the positions of the south and north parts of the host within the slit are slightly offset along a dispersion axis, although the two components are almost unresolved under actual observing condition as shown in Figure 1(a). This may cause, to some extent, a systematic difference of redshifts for each part of the spectrum. The spatial offset roughly corresponds to $\delta\lambda = 11\text{ \AA}$ on the detector, which is much less than the difference between the observed H α wavelengths in the south and north parts ($= 29\text{ \AA}$).

In order to measure emission-line fluxes, we performed spectral fitting analysis for each spectrum, assuming the redshift and line width shared between H α and [NII] λ 6584, their fluxes, and a constant continuum level as free parameters (Figure 4). For the north part, a single emission line and constant continuum are assumed. We used only the rest-frame wavelength range of 6400–6600 \AA for our fitting analysis to avoid noisy background at $\lambda > 6600\text{ \AA}$. Because the redshifted H α emission of the north part of the spectrum could contaminate the [NII] λ 6584 flux of the whole spectrum, we also analyzed the sum of the south and north parts of the spectra after shifting each spectrum to a common redshift based on the measured radial velocity offset of the H α line. The kinematic and morphological multiple components of the host galaxy are discussed in Section 4.3.

3. RESULTS

We estimated metallicities for each spectrum using the [NII] λ 6584/H α ratio based on the Pettini & Pagel (2004) method (hereafter PP04 N2). Since the absolute value of the metallicity derived from emission-line diagnostics depends on the calibration method (e.g., Kennicutt et al. 2003; Kewley & Ellison 2008), the metallicity comparison basically requires using an identical calibration. We adopt the Kobulnicky & Kewley (2004) method (hereafter KK04) as a common metallicity calibration to compare with other metallicity measurements. The PP04 N2 metallicity of the GRB 080325 host is converted to KK04 using the conversion formula parameterized by Kewley & Ellison (2008). The metallicities of the whole, south, and north parts of the spectra are $12 + \log(\text{O}/\text{H})_{\text{KK04}} = 8.88, 8.78$, and < 8.75 , respectively. Here, the assumed $12 + \log(\text{O}/\text{H})$ for the solar metallicity is ~ 8.7 (Allende Prieto et al. 2001; Asplund et al. 2004) for both calibrations (Kobulnicky & Kewley 2004; Pettini & Pagel 2004).

We also estimated the slit loss to be ~ 0.3 by smoothing the J -band *HST* image, i.e., $\sim 70\%$ of the total flux from the host is incident within the $0''.7$ slit (Figure 1). The extinction-corrected total SFR of the host is $35.6\text{--}47.0 M_{\odot} \text{ yr}^{-1}$ (see also Section 4.1), which is calculated from the H α luminosity using the conversion equation derived by Savaglio et al. (2009) and the slit loss.

We also performed a full re-analysis of both the Keck and Subaru optical photometry, using a common aperture radius of $1''.25$ and a common field calibration from the Palomar 60 inch telescope for every image. The updated ground-based optical photometry magnitudes are summarized in Table 1. We performed a new SED fit with these optical data (fixing the

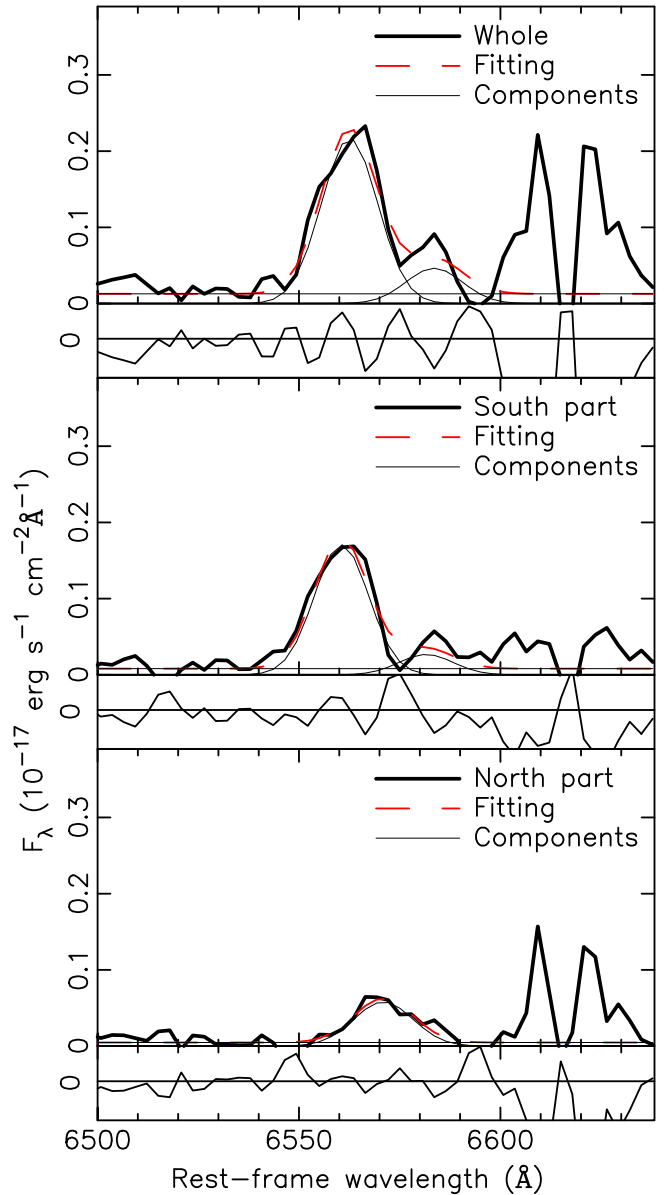


Figure 4. Spectral fits for spectra extracted from the whole, south, and north parts of the host galaxy of GRB 080325. The wavelength is converted to rest-frame given a redshift of $z = 1.78$, as derived from H α emission in the whole spectrum. Red dashed lines are best-fit models and thin solid lines are each of the model components. Residuals between observed spectra and best-fit models are shown at the bottom of each spectrum.

Table 1
Updated Ground-based Optical Photometry of the GRB 080325 Host Galaxy

Filter	Mag.	Error	System	Telescope
u'	25.91	0.25	SDSS	Keck/LRIS
B	25.75	0.12	Vega	Subaru/Suprime
g'	25.48	0.08	SDSS	Keck/LRIS
R	24.60	0.11	Vega	Keck/LRIS
R	24.63	0.14	Vega	Subaru/Suprime
i'	24.72	0.15	SDSS	Keck/LRIS
i'	24.67	0.20	SDSS	Subaru/Suprime
z'	24.18	0.09	SDSS	Subaru/Suprime

Note. Magnitudes are not corrected for Galactic extinction.

Table 2
Results of SED Fitting and Emission-line Fitting
Analysis of the GRB 080325 Host Galaxy

	Stellar Mass $\log(M_*/M_\odot)$	SFR _{SED} ^a ($M_\odot \text{ yr}^{-1}$)	$A_{V,\text{stellar}}$	
	$11.02^{+0.05}_{-0.09}$	$20.3^{+13.1}_{-9.5}$	$1.17^{+0.14}_{-0.17}$	
	H α flux $10^{-17} \text{ erg s}^{-1} \text{ cm}^{-2}$	[NII] $\lambda 6584$ flux $10^{-17} \text{ erg s}^{-1} \text{ cm}^{-2}$	Line FWHM (km s^{-1})	Velocity offset (km s^{-1})
Whole	10.6 ± 0.34	2.3 ± 0.31	508.4 ± 27.3	91.3
South part	8.0 ± 0.22	1.3 ± 0.19	465.8 ± 22.4	0.0
North part	3.0 ± 0.24	$< 0.39^c$	565.1 ± 65.5	474.5^d
South+North ^b	11.0 ± 0.34	2.3 ± 0.31	508.0 ± 21.0	...
	$12 + \log(\text{O}/\text{H})_{\text{KK04}}^e$ KK04 calibration	SFR _{Hα} ^f $M_\odot \text{ yr}^{-1}$	SFR _{Hα} ^g $M_\odot \text{ yr}^{-1}$	sSFR Gyr^{-1}
Whole	$8.88^{+0.05}_{-0.06}$	35.6 ± 1.1	47.0 ± 1.5	$0.34\text{--}0.45$
South part	$8.78^{+0.05}_{-0.06}$	27.0 ± 0.7	35.7 ± 1.0	
North part	< 8.75	10.0 ± 0.8	13.2 ± 1.0	$\sim 0.32^h$
South+North ^b	$8.70^{+0.06}_{-0.06}$	37.0 ± 1.0	49.0 ± 1.3	$0.36\text{--}0.47$

^a SFR derived from SED fitting of GRB 080325 host galaxy.

^b Sum of the south and north parts of the spectra, but the north spectra is blueshifted by 474.5 km s^{-1} .

^c 3σ upper limit.

^d The velocity offset could be $\sim 300 \text{ km s}^{-1}$ if the spatial offset of the two components within the slit is taken into account.

^e Metallicity based on the PP04 N2 method (Pettini & Pagel 2004) is converted to that for the KK04 method (Kobulnicky & Kewley 2004) using the conversion formula of Kewley & Ellison (2008) for comparison with other GRB host samples. The denoted errors do not include the systematic error (~ 0.1 dex) associated with metallicity calibration.

^f $A_{V,\text{emission}}$ identical to $A_{V,\text{stellar}}$ derived from the SED fitting analysis is assumed. The slit loss of ~ 0.3 is taken into account.

^g $A_{V,\text{emission}} = A_{V,\text{stellar}}/0.76$ (Zahid et al. 2014b) is assumed. The slit loss of ~ 0.3 is taken into account.

^h 40% of the total stellar mass is assumed for the north part component.

redshift to the spectroscopic value of $z = 1.78$) and NIR magnitudes reported in Hashimoto et al. (2010) and Perley et al. (2013), using a similar procedure as in Perley et al. (2013) but with a more flexible star formation history model. The best-fit result indicates that the host is a dusty ($A_V = 1.17$ mag), massive ($M_* \sim 10^{11} M_\odot$) star-forming galaxy, consistent with our previous estimates (Hashimoto et al. 2010; Perley et al. 2013). Metallicity, SFR, and other host properties derived from the SED fitting are summarized in Tables 2 and 3 for the whole, south, and north spectra as defined above. We also present our results for a summation of the south and north parts in which the north is blueshifted in wavelength to account for the velocity offset between the components.

4. DISCUSSION

4.1. Star Formation Rate

The total SFR calculated from the H α luminosity of the whole host galaxy (SFR_{H α}) is $14.7 M_\odot \text{ yr}^{-1}$ without any dust extinction correction if a slit loss of ~ 0.3 (see Section 2) is taken into account. The extinction-corrected SFR_{H α} is $35.6 M_\odot \text{ yr}^{-1}$

Table 3
Summary of $12 + \log(\text{O}/\text{H})$ Derived from Different Metallicity Calibrations

	PP04 N2 ^a	KK04 ^b	N06 ^c	FMR ^d
Whole	$8.48^{+0.06}_{-0.06}$	$8.88^{+0.05}_{-0.06}$	8.7	~ 9.0
South part	$8.39^{+0.05}_{-0.05}$	$8.78^{+0.05}_{-0.06}$
North part	< 8.36	< 8.75	< 8.52	~ 9.0

Notes. These values do not include the systematic error (~ 0.1 dex) associated with metallicity calibration.

^a PP04 N2 (Pettini & Pagel 2004) metallicity is calculated from observed [NII] $\lambda 6584/\text{H}\alpha$.

^b Metallicity based on the PP04 N2 method (Pettini & Pagel 2004) is converted to the KK04 method (Kobulnicky & Kewley 2004) using the conversion formula of Kewley & Ellison (2008) for comparison with other GRB host samples.

^c Metallicity based on the N06 (Nagao et al. 2006) method is calculated using coefficients of the best-fit polynomials for the observed relations between [NII] $\lambda 6584/\text{H}\alpha$ and the oxygen abundance of star-forming galaxies.

^d Expected metallicity from the FMR derived by Mannucci et al. (2010). Note that this value should be compared with the N06 (Nagao et al. 2006) calibration.

assuming a Calzetti et al. (2000) extinction law, given the dust extinction ($A_V = 1.17$ mag; Table 2) derived from SED fitting of the photometric data. This value is in agreement with the SFR estimated by the SED fitting (SFR_{SED} = $20.3^{+13.1}_{-9.5}$). However, the amount of extinction for the stellar component of a galaxy is not always the same as for the emission lines (e.g., Calzetti et al. 2000; Zahid et al. 2014b). If such a difference is taken into account (i.e., using an average correction factor of $A_{V,\text{emission}} = A_{V,\text{stellar}}/0.76$ at $z \sim 1.6$; Zahid et al. 2014b), then SFR_{H α} is estimated to be $47.0 M_\odot \text{ yr}^{-1}$. These SFRs are consistent with the distribution of other GRB host galaxies which show a wide range, e.g., from ~ 0.1 to $\sim 100 M_\odot \text{ yr}^{-1}$ at $z > 1$ (Figure 5). In the figure, the GRB sample is collected from the publicly available GHostS database;⁶ core-collapse supernovae are taken from Svensson et al. (2010) and Kelly et al. (2014). The top and bottom dashed lines show the redshift evolution of the SFR of those magnitude-selected star-forming galaxies with $\log(M_*/M_\odot) = 8.0$ and 11.5 (Whitaker et al. 2012), although the uncertainty is large at higher redshifts for less-massive galaxies. Because of the well-known correlation between SFR and stellar mass for star-forming galaxies (the so-called “star formation main sequence”; e.g., Brinchmann et al. 2004; Noeske et al. 2007), normal star-forming galaxies are distributed between two dashed lines. Our results imply that the SFR distribution of GRB host galaxies falls in the same range as for normal star-forming galaxies over a wide range of redshift up to ~ 1.8 .

Mannucci et al. (2011) demonstrated that the physical properties of GRB host galaxies are consistent with the fundamental metallicity relation (FMR) of normal star-forming galaxies—that is, the tight dependence of metallicity on stellar mass and SFR (Mannucci et al. 2010). They suggested that low metallicity is not necessarily important for a galaxy to host a GRB but that GRB production seems to be related to the efficiency of star formation as measured by the specific star formation rate (sSFR), the SFR normalized to the total stellar mass of the galaxy. In fact, previously researched low- z GRB

⁶ <http://www.grbhosts.org>

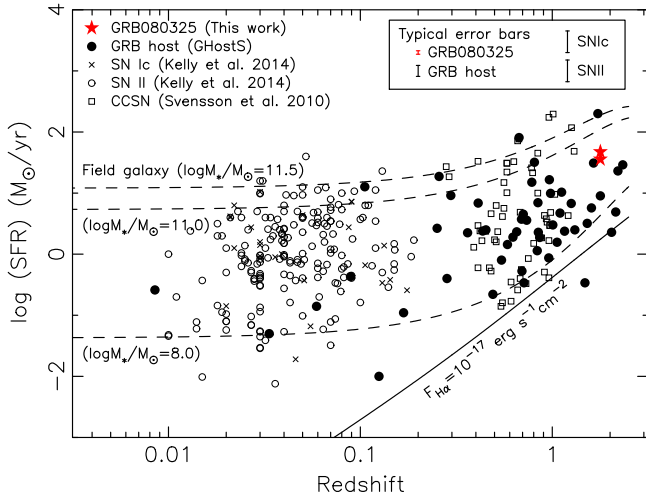


Figure 5. SFRs of GRB 080325 (red stars), assuming two cases of emission-line extinction of $A_{V,\text{emission}} = A_{V,\text{stellar}}$ and $A_{V,\text{emission}} = A_{V,\text{stellar}}/0.76$ (Zahid et al. 2014b) and other GRB hosts (black dots; GHostS project) as a function of redshift. The error bar of the GRB 080325 host is for each data point. For comparison, local core-collapse supernova hosts, i.e., type Ic (crosses) and II (open circle) hosts, are over plotted (Kelly et al. 2014) along with intermediate-redshift core-collapse supernova hosts (squares; Svensson et al. 2010). Three dashed lines correspond to the SFR of normal star-forming galaxies with stellar masses of $\log(M_*/M_\odot) = 8.0, 11.0$, and 11.5 , respectively (the star formation “main sequence”; Whitaker et al. 2012). The solid line is SFR calculated from the $H\alpha$ flux density, $f = 10^{-17} \text{ erg s}^{-1} \text{ cm}^{-2}$ as a reference of detection limit of $H\alpha$.

host galaxies are biased toward higher sSFR compared with local star-forming galaxies (e.g., Mannucci et al. 2011).

For the GRB 080325 host, the SFR is *lower* than for normal star-forming galaxies with stellar mass $\sim 10^{11} M_\odot$ at $z \sim 1.6$ (e.g., Kashino et al. 2013; see also the middle dashed line in Figure 5). This means that the sSFR of the host galaxy is lower than normal for star-forming galaxies at a fixed stellar mass. The sSFR of the host is $(0.34\text{--}0.45) \text{ Gyr}^{-1}$ (Table 2), which is likewise lower than the typical value of $\sim 1.0 \text{ Gyr}^{-1}$ for normal star-forming galaxies with the same stellar mass at $z \sim 1.6$ (Kashino et al. 2013). We also estimated the expected metallicity from the FMR derived by Mannucci et al. (2010) as follows:

$$12 + \log(\text{O}/\text{H})_{\text{FMR}} = 8.90 + 0.39x - 0.20x^2 - 0.077x^3 + 0.064x^4, \quad (1)$$

where $x = \mu_{0.32} - 10.0$ and $\mu_{0.32} = \log(M_*/M_\odot) - 0.32 \times \log(\text{SFR})$. The expected metallicity is $12 + \log(\text{O}/\text{H})_{\text{FMR}} \sim 9.0$ (Table 3). Even if the systematic metallicity calibration error (~ 0.1) is taken into account, this is higher than our spectroscopically measured value of $12 + \log(\text{O}/\text{H})_{\text{N06}} = 8.7$, as estimated from the $[\text{NII}]\lambda 6584/H\alpha$ ratio. Note that the Nagao et al. (2006) calibration (N06) is used here, in common with the calibration for $12 + \log(\text{O}/\text{H})_{\text{FMR}}$.

The GRB 080325 host therefore has relatively low sSFR and is an outlier from the FMR, in contrast with most low- z GRB host galaxies. The redshift dependence of the FMR is still under debate. Mannucci et al. (2010) reported that high-redshift galaxies up to $z \sim 2.5$ are found to follow the same FMR defined by local star-forming galaxies with no indication of evolution. Hunt et al. (2012) also found that the correlations between metallicity, stellar mass, and SFR for star-forming

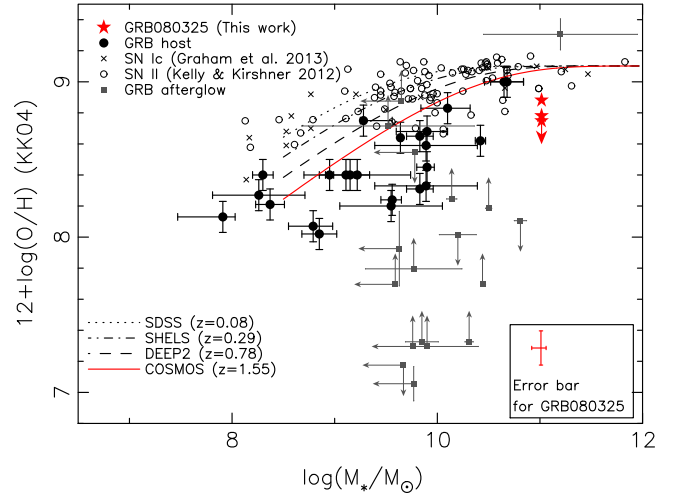


Figure 6. Mass–metallicity relation of GRB host galaxies. The red star is the metallicity of the GRB 080325 host galaxy (this work). Beginning at the top, the three stars correspond to metallicities estimated from the Whole, south, and north part spectra, respectively. Black dots are GRB host samples mainly collected by Levesque (2014), supplemented by stellar mass derived by Svensson et al. (2010) and Schulze et al. (2014) with additional samples of GRB 011121 (Svensson et al. 2010; Graham & Fruchter 2013), GRB 060505 (Thöne et al. 2008; Graham & Fruchter 2013), GRB 080605 (Krühler et al. 2012), GRB 100418A (Niino et al. 2012), GRB 110918A (Elliott et al. 2013), GRB 120422A (Schulze et al. 2014), and 121024A (Friis et al. 2014). Filled squares are absorption-line metallicities of GRB afterglows at $z < 4$ collected by Cucchiara et al. (2014) with the stellar mass from GHostS and Laskar et al. (2011). Each curved line shows the mass–metallicity relation for normal star-forming galaxies at each redshift (Zahid et al. 2014a). Error bars include fitting errors and the typical systematic error of metallicity calibration ~ 0.1 dex (Kewley & Ellison 2008).

galaxies are generally redshift-invariant (up to ~ 3.5). On the other hand, some differences in the FMR, more or less, between local and high-redshift galaxies ($z \sim 1.4$ and 1.6) are reported (Yabe et al. 2012, 2014; Zahid et al. 2014b). Niino (2012) demonstrated a redshift evolution of the FMR within narrow redshift bins based on local star-forming galaxy samples. Anyway, our results for the GRB 080325 host suggests that the presumption of Mannucci et al. (2011), i.e., that high star-forming efficiency plays an important role in the production of GRBs rather than low metallicity, is not always applicable to high- z GRB hosts as long as we assume the FMR by Mannucci et al. (2010).

4.2. Metallicity of the GRB 080325 Host

The host galaxy of GRB 080325 is one of the most massive and distant host galaxies for which a metallicity has been determined through emission-line diagnostics (see Section 3 and Table 2 for the detailed description of metallicity measurement). This metallicity should be compared with other galaxies at similar high redshifts when the cosmic SFR density was at its peak, in contrast to previous GRB host emission-line studies, nearly all of which are at $z < 1.0$ (except for GRB 080605 at $z = 1.64$, Krühler et al. 2012; and GRB 121024A at $z = 2.3$, Friis et al. 2014). Figure 6 shows the mass–metallicity relation for a sample of GRB host galaxies; observations were mainly collected by Levesque (2014) and supplemented with stellar masses derived by Svensson et al. (2010) and Schulze et al. (2014). We added to this GRB 011121 (Svensson et al. 2010; Graham & Fruchter 2013), GRB 060505 (Thöne et al. 2008; Graham & Fruchter 2013), GRB 080605 (Krühler

et al. 2012), GRB 100418A (Niino et al. 2012), GRB 110918A (Elliott et al. 2013), GRB 120422A (Schulze et al. 2014), and 121024A (Friis et al. 2014) as well as the GRB 080325 host galaxy (this paper). Although the possibility of a systematic offset between metallicities derived from emission-line diagnostics and absorption-line systems of GRB afterglow is still unclear, absorption-line metallicities at $z < 4$ are also shown in the figure for reference (metallicity measurements from Cucchiara et al. 2014 and stellar masses from GHostS and Laskar et al. 2011.) For comparison, nearby type Ic and II supernova host galaxies (Kelly & Kirshner 2012; Graham & Fruchter 2013; Kelly et al. 2014) are also denoted as well as the mass–metallicity relations of normal star-forming galaxies at various redshifts (Zahid et al. 2014a). All stellar masses in the figure are converted as necessary using a Chabrier (2003) initial mass function and all metallicities are based on the KK04 method. The GRB 080325 host is among the highest metallicity in GRB samples. This result suggests a disagreement with the presence of a critical cutoff above which GRBs cannot occur (as proposed by, e.g., Modjaz et al. 2008), even in the high-redshift universe. The metal-rich nature of the host in GRB samples also seems not to match up with the low-metallicity requirement suggested from theoretical modeling of single massive stellar evolution (e.g., Yoon et al. 2006; Woosley & Heger 2006). One possible way to explain high-metal GRB hosts is an alternate progenitor scenario, such as a binary system (Nomoto et al. 1995; Fryer et al. 1999; Iwamoto et al. 2000) or magnetar. Recently, the idea of gradual metallicity-dependent biases has been proposed rather than a sharp metallicity cutoff, e.g., combination with a channel based on the evolution of single massive stars, where low-metallicity plays a crucial role as well as alternative channels without strong metallicity dependence (Trenti et al. 2013, 2014). As another possibility, we note that the metallicity measurement does not always reflect the immediate environment of the GRB (even in spatially resolved spectra such as ours) due to spectroscopic dilution by limited spatial resolution and poor S/N unless at least spatial resolution of ~ 500 pc is achieved (Niino et al. 2014). Such a requirement is not easy for high-redshift GRBs, even if the GRB-site spectrum is extracted from the host. There is an indication that the metallicity upper limit for the GRB 080325 site is lower than the metallicity of the whole host, but the spatial resolution is not high enough to examine the immediate environment of the GRB. The *HST* image suggests that the host system may be a major merger (see Section 4.3 for the detailed discussion) in which the GRB is associated with a northern stellar component. Because of this situation, the discovery of a high-metal host does not rule out a locally low-metal environment around the GRB.

The GRB 080325 host is metal-rich but its metallicity is still lower than for normal star-forming galaxies at similar redshifts (i.e., the COSMOS sample denoted by a red solid line). The redshift evolution of the mass–metallicity relation (e.g., Savaglio et al. 2005; Yabe et al. 2012, 2014; Zahid et al. 2014a) and the wide redshift distribution of the GRB sample often make this kind of comparison confusing. To clarify this, we adopt the stellar mass normalized by M_o , the turnover mass of the mass–metallicity relation proposed by Zahid et al. (2014a), above which the metallicity asymptotically approaches the upper limit. Here, $\log(M_o/M_\odot)$ is 9.12, 9.52, 9.81, and 10.11 for SDSS ($z = 0.08$; Abazajian et al. 2009), SHELs ($z = 0.29$; Geller et al. 2005), DEEP2

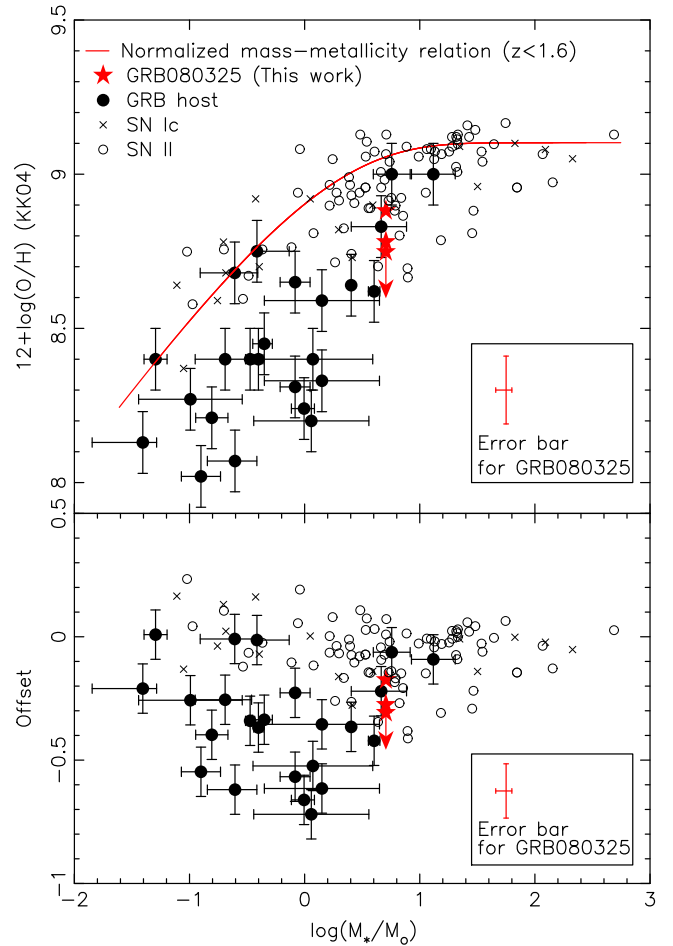


Figure 7. Same as Figure 6, but the galaxy stellar mass is normalized by M_o and the displayed sample is limited to $z < 2.0$ because M_o is calculated for the $z \lesssim 2$ sample by Zahid et al. (2014a; top). M_o is the characteristic turnover mass of the mass–metallicity relation, above which the metallicity asymptotically approaches the upper limit. The red solid line is the normalized-mass metallicity relation for normal star-forming galaxies at $z < 1.6$ (Zahid et al. 2014a). The offset metallicity of the GRB sample is defined relative to the normalized mass–metallicity relation (bottom).

($z = 0.78$; Davis et al. 2003), and COSMOS ($z = 1.55$; Zahid et al. 2014b) surveys, respectively. They clearly demonstrated the mass–metallicity relation at $z < 1.6$ is fairly independent of redshift if a normalized galaxy stellar mass is used. They also showed that M_o as a function of redshift is well fit by a linear function as follows.:

$$\log(M_o/M_\odot) = (9.138 \pm 0.003) + (2.64 \pm 0.05) \times \log(1 + z). \quad (2)$$

The stellar mass of Figure 6 is converted to mass in the M_o unit by using Equation (2), slightly extrapolating this relation to $z = 1.78$. The normalized mass–metallicity relation is shown in Figure 7. The relation for the SDSS, SHELs, DEEP2, and COSMOS samples is drawn by an identical line in the figure because the redshift evolution between the samples has largely been removed by the M_o correction. The distribution of the core-collapse supernova hosts is consistent with the distribution of normal star-forming galaxies. On the other hand, GRB host galaxies including the GRB 080325 host are clearly below the normalized mass–metallicity relation. The offset metallicity (which we define as the difference between the observed

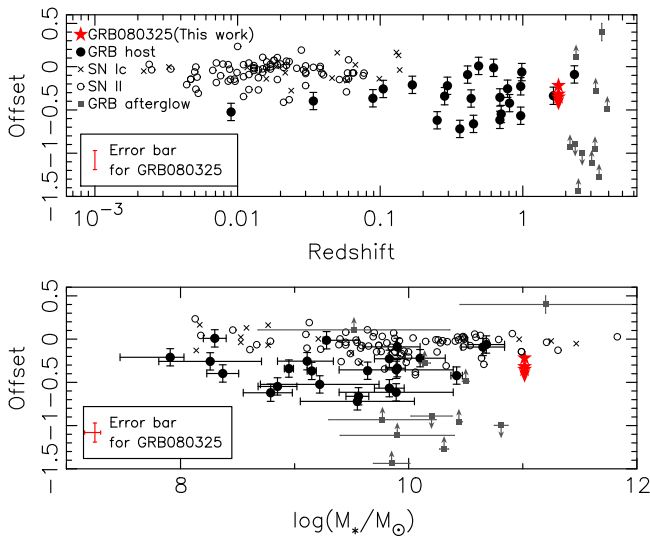


Figure 8. Offset metallicity from normalized-mass metallicity relation as a function of redshift (top) and stellar mass (bottom). Symbols are the same as in Figure 6. Note that the offsets for the GRB 121024A host and absorption-line metallicities at $z < 4$ are estimated by comparison with the mass–metallicity relation of star-forming galaxies at $z = 2.3\text{--}3.5$ (Maiolino et al. 2008; Steidel et al. 2014). Among the absorption metallicities collected in the Cucchiara et al. (2014) sample, only host galaxies with known stellar mass are plotted.

metallicity and the metallicity expected given the host stellar mass assuming a normalized mass–metallicity relation) is shown in the bottom of the figure. The offset of the GRB 080325 host is rather close to the typical value of the GRB sample. The distribution of GRB hosts is ~ 0.4 dex lower than normal star-forming galaxies without any clear dependency on normalized stellar mass. This indicates that GRBs preferably occur in low-metal galaxies, uniformly biased toward typically ~ -0.4 dex regardless of both redshift and host galaxy stellar mass. This tendency is also demonstrated in Figure 8, which shows the metallicity offset as a function of redshift and stellar mass. While a direct comparison with emission-line and absorption-line metallicities probably includes large uncertainties, offsets for GRB absorption-line metallicity measurements at $z < 4$ are also shown in the figure for reference (that is, the offset from the mass–metallicity relation for star-forming galaxies at $z = 2.3\text{--}3.5$ from Maiolino et al. 2008.) There is no significant correlation between metallicity offset and redshift or between metallicity offset and stellar mass for GRB host galaxies, even if absorption-line metallicities based on GRB afterglows are included. This result supports the conclusions of Levesque et al. (2010a), who reported a mass–metallicity relation for GRB host galaxies shifted toward low metallicity by -0.42 dex (where they simply divided their sample into two redshift categories, i.e., $z < 0.3$ and $0.3 < z < 1.0$). We also emphasize that GRB 080325 is an important case demonstrating that a GRB can occur in a low-metal galaxy compared with normal star-forming galaxies of the same mass in a similar manner to local GRBs, even in the high-redshift (beyond $z \sim 1$) universe. We conclude that the low-metallicity nature of the GRB 080325 host is probably not attributable to the FMR of star-forming galaxies because the host is an outlier of the relationship as discussed in Section 4.1; rather, the metallicity itself is probably essential for the production mechanism of this GRB. Recently, Perley et al. (2014) presented observations of a uniformly selected sample of GRB

hosts with high radio star formation rates ($50\text{--}200 M_{\odot} \text{ yr}^{-1}$, similar to ultra-luminous infrared galaxies and submillimeter galaxies). The GRB hosts in this subset have lower stellar masses and higher specific star formation rates than field galaxies of similar IR/submillimeter/radio luminosity, even though the fraction of radio-luminous hosts identified in their sample (15%) is consistent with the fraction of star formation thought to occur in such galaxies. They suggest that the GRB rate may depend independently on both metallicity (the GRB rate is suppressed in high-metallicity environments) and star formation efficiency (the GRB rate is enhanced in regions of high specific star formation). The GRB 080325 host shows that this need not be true for every case: while its metallicity is relatively low compared to other galaxies of the same mass, its specific SFR is modest.

According to spectroscopic surveys of high-redshift star-forming galaxies, there are indications that distant star-forming galaxies occupy a region of the BPT plane (Baldwin et al. 1981) distinct from star-forming galaxies in the local universe (e.g., Shapley et al. 2005; Erb et al. 2006; Yabe et al. 2012, 2014; Steidel et al. 2014). A similar situation is also reported for galaxies with intense star formation at low redshifts (e.g., Jaskot & Oey 2013; Stanway et al. 2014), suggesting that it could be an sSFR effect. Recently, results from an extensive spectroscopic survey of high-redshift galaxies at $2.0 < z < 2.6$ have been reported by Steidel et al. (2014). They suggest that high-redshift galaxies have harder stellar ionizing radiation, a higher ionization parameter, and a shallower dependence of N/O on O/H than is typically inferred for galaxies in the local universe. Anyway, it is not clear whether the metallicity calibrations based on HII regions in the local universe can be applied to the high-redshift universe or galaxies with high sSFR in general. It is actually found that the oxygen abundance of the PP04 N2 method is systematically higher than that of the PP04 O3N2 method for high-redshift galaxies (Yabe et al. 2014; Steidel et al. 2014), which could result from systematically higher N/O at a given O/H in the high-redshift sample, as discussed by Steidel et al. (2014). We note that the sSFR of the GRB 080325 host is lower than that of normal star-forming galaxies at similar redshift, and our observations of the host are still indicative of low metallicity, even if the N2 method gives systematically higher oxygen abundances in the high-redshift universe.

While many of our conclusions are based on the analysis of a marginal detection of the [NII] $\lambda 6584$ emission line, we emphasize that the conclusions all still hold even if the [NII] $\lambda 6584$ detection of the GRB 080325 host is treated as an upper limit. The host still shows moderate SFR, low sSFR, and low metallicity compared with normal star-forming galaxies with the same mass at $z \sim 1.6$.

4.3. Two Components of the Host Galaxy?

As shown in Figure 2, the H α emission from the north component of the host galaxy is redshifted by 474.5 km s^{-1} relative to the south part. This velocity offset is rather higher than a typical galactic rotation velocity at $z \sim 2$ (e.g., Förster Schreiber et al. 2009), suggesting a merging system of multiple galaxies. In fact, the *J*-band image (rest-frame $\sim 4400 \text{ \AA}$; Figure 1) obtained by *HST* shows a double-peaked stellar component within the host. The position of the north stellar component in the *HST* image roughly corresponds to the north part of the spectrum which we defined kinematically. If this

GRB occurred in the merging system of two galaxies, then the GRB is likely hosted by the north stellar component (although the possibility that it occurred in the northern edge of the south stellar component cannot be excluded). Considering this situation, the stellar mass of the “true” host could be less massive than the total stellar mass of the combined system, which would make the discussion in Sections 4.1 and 4.2 more complicated. In order to roughly estimate the individual stellar mass of the north component we divided the *HST* *J*-band image of the host into two components and measured a light fraction of the north component. This fraction is $\sim 40\%$ of the total light in the *J* band, which suggests that a comparable fraction of the total stellar mass is also in this component. Given this mass for the north stellar component and our earlier measurement of the SFR for the north part spectrum, the sSFR inferred for the north component is 0.32 Gyr^{-1} , which is still lower than typical star-forming galaxies at similar redshift (e.g., Whitaker et al. 2012). In a similar way, the upper limit on the metallicity derived from the north part of the spectrum is $12 + \log(\text{O}/\text{H}) = 8.52$ (N06 calibration for comparison with the FMR metallicity) or 8.75 (KK04 calibration in Figure 6). Even if the typical metallicity calibration error (~ 0.1) is taken into account, this is also lower than the metallicity inferred from the FMR (~ 9.0) or normalized mass–metallicity relation ($= 8.98$ in Figure 6) of normal star-forming galaxies, calculated using the north part of the SFR and stellar mass (Table 3).

Finally, we comment on the possibility of misidentification of the emission lines. We first note that the photometric redshift of $1.8 < z_{\text{phot}} < 2.2$ (Hashimoto et al. 2010) rules out the association of our putative $\text{H}\alpha$ line with any other strong nebular emission lines at different redshifts: specifically, the cases of $[\text{OIII}]\lambda 5007$ for a galaxy at $z = 2.65$, $[\text{OIII}]\lambda 4959$ at $z = 2.68$, $\text{H}\beta$ at $z = 2.76$, and $[\text{OII}]\lambda 3727$ at $z = 3.90$ are all strongly excluded by the photometric fit; the strong *U* and *B* detections in particular give no suggestion of a break indicating the onset of the $\text{Ly}\alpha$ forest as expected for a higher-redshift galaxy. The marginal detection of $[\text{NII}]\lambda 6584$ at the correct wavelength further supports our preferred redshift. It is possible, although statistically very unlikely, that the north component may represent a background galaxy at one of these alternate redshifts behind an unrelated object at $z = 1.78$; our photometric analysis would not be able to rule this out since the two objects are strongly blended, except in *HST* imaging. However, even in this case, we would expect to detect additional lines elsewhere in our spectral coverage; in particular, if it were to be one member of $[\text{OIII}]\lambda 5007$, $[\text{OIII}]\lambda 4959$, or $\text{H}\beta$, then we would expect to observe the other lines (as well as $[\text{OII}]\lambda 3727$) but in all cases do not. In the case of $[\text{OII}]\lambda 3727$ at $z = 3.90$, all other expected strong nebular emission lines are out of range, but the chance of a sub-arcsecond positional association of two galaxies with a redshift offset precisely tuned to align two unrelated emission lines in observed wavelength nevertheless is extremely remote. We therefore conclude that the emission line detected in the north spectrum is likely $\text{H}\alpha$ from a galaxy component physically associated with the south component of the host.

Thus, we conclude that the kinematic and morphological complexity of the host does not significantly affect discussions on the low-metallicity nature of GRB hosts in Sections 4.1 and 4.2.

5. SUMMARY

We detected the $\text{H}\alpha$ and $[\text{NII}]\lambda 6584$ emission lines of the host galaxy of the dark GRB 080325 using Subaru/MOIRCS. The host is a massive ($\sim 10^{11} M_{\odot}$), dusty ($A_V = 1.17 \text{ mag}$) star-forming galaxy at $z = 1.78$, in contrast with blue less-massive GRB host galaxies in the local universe.

The SFR indicated from $\text{H}\alpha$ is between 35.6 and $47.0 M_{\odot} \text{ yr}^{-1}$ (depending on the ratio of emission-line extinction to stellar extinction), consistent with the SFR derived from SED fitting of the photometry. This value is typical among GRB host galaxies and implies that the SFRs of GRB host galaxies are distributed similarly to those of normal star-forming galaxies over a wide range of redshift up to at least $z \sim 1.8$. On the other hand, the sSFR of the host is lower than normal for star-forming galaxies, in contrast with the high sSFR nature observed for many other GRB host galaxies. In addition, the expected host metallicity calculated from the FMR of normal star-forming galaxies is higher than the actual metallicity measurement obtained using emission-line diagnostics, even if the systematic error of the metallicity calibration is taken into account. The GRB 080325 host is therefore both an outlier from the FMR (with a lower metallicity than expected given its mass and SFR) and has a low sSFR. Although the evolution of the FMR is still under discussion, this result suggests that the previous presumption of the importance of high star-forming efficiency rather than low metallicity as the primary condition needed to produce a GRB is not in agreement with this case.

The host metallicity derived from $[\text{NII}]\lambda 6584/\text{H}\alpha$ is fairly high compared to GRB host galaxies at lower redshift, providing evidence against the existence of a critical metallicity cutoff above which GRBs never occur. Even if the cutoff existed, it is much higher than that suggested for low- z GRB host galaxies. This may favor progenitor scenarios other than the canonical single-star model, such as models involving a binary system or magnetar. Another possibility is spectroscopic dilution due to limited spatial resolution. Actually, there is a hint of a local low-metal environment, i.e., the upper limit of the metallicity at the GRB-site is lower than that for the whole host galaxy, although the spatial resolution is not enough to investigate the specific HII region in which the GRB occurred.

In any case, the metallicity of the host is still lower than normal for massive star-forming galaxies at $z \sim 1.6$. To avoid confusion due to the wide redshift range of the current GRB sample and the redshift evolution of the mass–metallicity relation for normal star-forming galaxies, we adopted a normalized mass–metallicity relation that is independent of redshift. The metallicity offset of the host from the normalized mass–metallicity relation is $\lesssim -0.2$ dex, which is close to the typical value of other GRB hosts. We also found that the metallicity offset distribution for GRB hosts is uniformly biased toward low metallicity regardless of redshift ($0 < z < 1.8$) and stellar mass ($10^8 < M_*/M_{\odot} < 10^{11}$), compared with core-collapse supernova host galaxies. GRB 080325 is an important case of a GRB occurring in a galaxy that is metal-poor compared with normal star-forming galaxies, even though it is a massive galaxy and even though it is at relatively high redshift. We emphasize that the low-metallicity nature of GRB 080325 is likely not attributable to the FMR of star-forming galaxies since this is an outlier of the FMR, i.e., low metallicity (not high sSFR) is likely essential for this burst.

We thank the Subaru Telescope staff for their invaluable help for our observation with Subaru/MOIRCS. Work by T.H. was supported by funding from the National Astronomical Observatory of Japan and the TMT project office in Japan. T.H. acknowledges the Department of Astronomy, California Institute of Technology for providing an excellent academic research environment for writing the paper and also thanks S. R. Kulkarni and T. Usuda for creating the opportunity for this collaborative study.

REFERENCES

- Abazajian, K. N., Adelman-McCarthy, J. K., Agüeros, M. A., et al. 2009, *ApJS*, **182**, 543
- Allende Prieto, C., Lambert, D. L., & Asplund, M. 2001, *ApJL*, **556**, L63
- Asplund, M., Grevesse, N., Sauval, A. J., Allende Prieto, C., & Kiselman, D. 2004, *A&A*, **417**, 751
- Baldwin, J. A., Phillips, M. M., & Terlevich, R. 1981, *PASP*, **93**, 5
- Bennett, C. L., Larson, D., Weiland, J. L., et al. 2013, *ApJS*, **208**, 20
- Berger, E., Fox, D. B., Kulkarni, S. R., Frail, D. A., & Djorgovski, S. G. 2007, *ApJ*, **660**, 504
- Brinchmann, J., Charlot, S., White, S. D. M., et al. 2004, *MNRAS*, **351**, 1151
- Calzetti, D., Armus, L., Bohlin, R. C., et al. 2000, *ApJ*, **533**, 682
- Chabrier, G. 2003, *PASP*, **115**, 763
- Cucchiara, A., Fumagalli, M., Rafelski, M., et al. 2014, arXiv:1408.3578
- Davis, M., Faber, S. M., Newman, J., et al. 2003, *Proc. SPIE*, **4834**, 161
- Elliott, J., Krühler, T., Greiner, J., et al. 2013, *A&A*, **556**, A23
- Erb, D. K., Shapley, A. E., Pettini, M., et al. 2006, *ApJ*, **644**, 813
- Förster Schreiber, N. M., Genzel, R., Bouché, N., et al. 2009, *ApJ*, **706**, 1364
- Friis, M., De Cia, A., Krühler, T., et al. 2014, arXiv:1409.6315
- Fryer, C. L., Woosley, S. E., & Hartmann, D. H. 1999, *ApJ*, **526**, 152
- Geller, M. J., Dell’Antonio, I. P., Kurtz, M. J., et al. 2005, *ApJL*, **635**, L125
- Graham, J. F., & Fruchter, A. S. 2013, *ApJ*, **774**, 119
- Hashimoto, T., Ohta, K., Aoki, K., et al. 2010, *ApJ*, **719**, 378
- Hayashi, M., Motohara, K., Shimasaku, K., et al. 2009, *ApJ*, **691**, 140
- Hunt, L., Magrini, L., Galli, D., et al. 2012, *MNRAS*, **427**, 906
- Hunt, L., Palazzi, E., Rossi, A., et al. 2011, *ApJL*, **736**, L36
- Ichikawa, T., Suzuki, R., Tokoku, C., et al. 2006, *Proc. SPIE*, **6269**, 38
- Iwamoto, K., Nakamura, T., Nomoto, K., et al. 2000, *ApJ*, **534**, 660
- Jakobsson, P., Hjorth, J., Fynbo, J. P. U., et al. 2004, *ApJL*, **617**, L21
- Jaskot, A. E., & Oey, M. S. 2013, *ApJ*, **766**, 91
- Kashino, D., Silverman, J. D., Rodighiero, G., et al. 2013, *ApJL*, **777**, L8
- Kawai, N., Kosugi, G., Aoki, K., et al. 2006, *Natur*, **440**, 184
- Kelly, P. L., Filippenko, A. V., Modjaz, M., & Kocevski, D. 2014, *ApJ*, **789**, 23
- Kelly, P. L., & Kirshner, R. P. 2012, *ApJ*, **759**, 107
- Kennicutt, R. C., Jr., Bresolin, F., & Garnett, D. R. 2003, *ApJ*, **591**, 801
- Kewley, L. J., & Ellison, S. L. 2008, *ApJ*, **681**, 1183
- Kobulnicky, H. A., & Kewley, L. J. 2004, *ApJ*, **617**, 240
- Krühler, T., Fynbo, J. P. U., Geier, S., et al. 2012, *A&A*, **546**, A8
- Krühler, T., Greiner, J., Schady, P., et al. 2011, *A&A*, **534**, A108
- Laskar, T., Berger, E., & Chary, R.-R. 2011, *ApJ*, **739**, 1
- Le Floch, E., Duc, P.-A., Mirabel, I. F., et al. 2003, *A&A*, **400**, 499
- Levesque, E. M. 2014, *PASP*, **126**, 1
- Levesque, E. M., Kewley, L. J., Berger, E., & Zahid, H. J. 2010a, *AJ*, **140**, 1557
- Levesque, E. M., Kewley, L. J., Graham, J. F., & Fruchter, A. S. 2010b, *ApJL*, **712**, L26
- Maiolino, R., Nagao, T., Grazian, A., et al. 2008, *A&A*, **488**, 463
- Mannucci, F., Cresci, G., Maiolino, R., Marconi, A., & Gnerucci, A. 2010, *MNRAS*, **408**, 2115
- Mannucci, F., Salvaterra, R., & Campisi, M. A. 2011, *MNRAS*, **414**, 1263
- Modjaz, M., Kewley, L., Kirshner, R. P., et al. 2008, *AJ*, **135**, 1136
- Nagao, T., Maiolino, R., & Marconi, A. 2006, *A&A*, **459**, 85
- Niino, Y. 2011, *MNRAS*, **417**, 567
- Niino, Y. 2012, *ApJ*, **761**, 126
- Niino, Y., Hashimoto, T., Aoki, K., et al. 2012, *PASJ*, **64**, 115
- Niino, Y., Nagamine, K., & Zhang, B. 2014, arXiv:1408.7059
- Noeske, K. G., Weiner, B. J., Faber, S. M., et al. 2007, *ApJL*, **660**, L43
- Nomoto, K. I., Iwamoto, K., & Suzuki, T. 1995, *PhRv*, **256**, 173
- Perley, D. A., Levan, A. J., Tanvir, N. R., et al. 2013, *ApJ*, **778**, 128
- Perley, D. A., Perley, R. A., Hjorth, J., et al. 2014, arXiv:1407.4456
- Pettini, M., & Pagel, B. E. J. 2004, *MNRAS*, **348**, L59
- Racusin, J. L., Karpov, S. V., Sokolowski, M., et al. 2008, *Natur*, **455**, 183
- Salvaterra, R., Della Valle, M., Campana, S., et al. 2009, *Natur*, **461**, 1258
- Savaglio, S., Glazebrook, K., & Le Borgne, D. 2009, *ApJ*, **691**, 182
- Savaglio, S., Glazebrook, K., Le Borgne, D., et al. 2005, *ApJ*, **635**, 260
- Schulze, S., Malesani, D., Cucchiara, A., et al. 2014, *A&A*, **566**, A102
- Shapley, A. E., Coil, A. L., Ma, C.-P., & Bundy, K. 2005, *ApJ*, **635**, 1006
- Stanek, K. Z., Gnedin, O. Y., Beacom, J. F., et al. 2006, *AcA*, **56**, 333
- Stanway, E. R., Eldridge, J. J., Greis, S. M. L., et al. 2014, *MNRAS*, **444**, 3466
- Stanway, E. R., Levan, A. J., Tanvir, N., et al. 2015, *MNRAS*, **446**, 3911
- Steidel, C. C., Rudie, G. C., Strom, A. L., et al. 2014, *ApJ*, **795**, 165
- Suzuki, R., Tokoku, C., Ichikawa, T., et al. 2008, *PASJ*, **60**, 1347
- Svensson, K. M., Levan, A. J., Tanvir, N. R., Fruchter, A. S., & Strolger, L.-G. 2010, *MNRAS*, **405**, 57
- Svensson, K. M., Levan, A. J., Tanvir, N. R., et al. 2012, *MNRAS*, **421**, 25
- Tanaka, I., Pyo, T.-S., Hattori, T., et al. 2008, GCN Circular, **7524**, 1
- Tanvir, N. R., Fox, D. B., Levan, A. J., et al. 2009, *Natur*, **461**, 1254
- Thöne, C. C., Fynbo, J. P. U., Östlin, G., et al. 2008, *ApJ*, **676**, 1151
- Tremonti, C. A., Heckman, T. M., Kauffmann, G., et al. 2004, *ApJ*, **613**, 898
- Trenti, M., Perna, R., & Jimenez, R. 2014, arXiv:1406.1503
- Trenti, M., Perna, R., & Tacchella, S. 2013, *ApJL*, **773**, L22
- Whitaker, K. E., van Dokkum, P. G., Brammer, G., & Franx, M. 2012, *ApJL*, **754**, L29
- Woosley, S. E., & Heger, A. 2006, *ApJ*, **637**, 914
- Yabe, K., Ohta, K., Iwamuro, F., et al. 2012, *PASJ*, **64**, 60
- Yabe, K., Ohta, K., Iwamuro, F., et al. 2014, *MNRAS*, **437**, 3647
- Yoon, S.-C., Langer, N., & Norman, C. 2006, *A&A*, **460**, 199
- Zahid, H. J., Dima, G. I., Kudritzki, R.-P., et al. 2014a, *ApJ*, **791**, 130
- Zahid, H. J., Kashino, D., Silverman, J. D., et al. 2014b, *ApJ*, **792**, 75